



Effects of ultrasonic vibration on the iron-containing intermetallic compounds of high silicon aluminum alloy with 2% Fe

Gu Zhong, Shusen Wu*, Huawen Jiang, Ping An

State Key Lab of Materials Processing and Die & Mould Technology, Huazhong University of Science and Technology, Luoyu Road 1037#, Wuhan 430074, PR China

ARTICLE INFO

Article history:

Received 31 August 2009

Received in revised form

19 November 2009

Accepted 19 November 2009

Available online 24 November 2009

Keywords:

Ultrasonic vibration

High silicon aluminum alloy

Iron-containing phase

Microstructure

ABSTRACT

The effects of ultrasonic vibration (USV), the combined effects of USV and the addition of Mn on the morphology of iron-containing intermetallic compounds of Al–20Si–2.0Fe–2.0Cu–0.4Mg–1.0Ni alloy have been studied respectively. The mechanism of shape-transformation of Fe-containing phases is also investigated. A large amount of long needle-like β -Al₅FeSi phases accompanied with a few δ -Al₄FeSi₂ phases existed in the matrix of high silicon aluminum alloy with 2% Fe in traditional casting process. The effects of acoustic cavitation and acoustic streaming generated by USV which was applied near the liquidus temperature of this alloy, homogenized the solute distribution field and temperature field of the melt, lowered the concentration level of Fe atoms in solidification front, and decreased the start-freezing temperature of β phase. That the formation of acicular β phase was suppressed, contribute to enlarge the forming temperature range of δ phase of the alloy with certain time of USV imposed near the liquidus temperature. The finest δ particles and only a small amount of β phase were obtained in the matrix of the Fe-containing alloy with USV for 120 s. With the complex effects of USV and addition of 0.5% Mn, the forming of acicular β phase was almost repressed and the Fe-containing phases were in forms of fine Al₄(Fe,Mn)Si₂ and Al₅(Fe,Mn)Si particles in the size of 20–30 μ m.

Crown Copyright © 2009 Published by Elsevier B.V. All rights reserved.

1. Introduction

High silicon (Si: 18–26%) Al–Si alloy has been considered to be an ideal candidate for making such heat- and wear-resistant parts as pistons of high speed engines, due to the superior performances of high specific strength, excellent wear resistance and corrosion resistance, as well as low coefficient of thermal expansion [1–3]. Generally, alloy elements, such as Cu, Mg, were added deliberately to improve the room temperature strength substantially by solution and precipitation hardening. However, strengthening phases like Al₂Cu and Al₂CuMg are relatively stable below 150 °C, and Mg₂Si will aggregate and coarsen over 180 °C that give rise to sharp decrease of high temperature strength [1]. It has been proved that addition of alloy element Fe was effective to enhance elevated mechanical properties through forming Fe-containing intermetallic compounds which are still stable at temperature of 300–400 °C [1,4–7]. Unfortunately, conventional casting technologies produce coarse plate Fe-bearing intermetallic compounds like β -Al₅FeSi and δ -Al₄FeSi₂, resulting in inferior mechanical properties.

In recent years, processes of modifying the harmful Fe-bearing intermetallic compounds by rapid solidification [1,5–7], neutraliza-

tion elements addition [1,6,7] and melt superheating were widely studied. With the addition of Mn according to certain ratio of Mn/Fe, the coarse plate β phase transforms to less detrimental Chinese script Al₁₅(Fe,Mn)₃Si₂ phase [7]. However, increase of Mn content can not only eliminate the harmful effect of β phase completely, but also cause high cost and inferior cutting performance for the high hardness polygonal α -Al₁₅(Fe,Mn)₃Si₂ phase formed [7–9]. Currently, rapid solidification techniques like spray forming process which produce fine microstructure, attract considerable interests. Fine δ -Al₄FeSi₂ phase in the size of 1.4–7.7 μ m of Al–20Si–5Fe–2X (X = Cu, Ni, Cr) alloy was obtained through gas atomization, contributing to the hardness increase about 7–17% [6]. The alloys prepared by spray deposition [1,7] which presented fine δ and β phases about 3–8 μ m, showed excellent strength at room temperature and elevated temperature. However, the expensive equipment and complicated process restricted the applications of this process in industry greatly.

USV was employed in the field of metal's semi-solid processing in continuously casting since 1990s. And the process of semi-solid slurry preparation by ultrasonic vibration now has attracted considerable concerns for the unique merits such as low cost and high efficiency, simple process, and little pollution to melt and environment [10–12]. Currently, the refine mechanism of the α -Al dendrites [10,11] and primary Si particles [3,12], as well as the effects of process parameters [11] on refinement are the main

* Corresponding author. Tel.: +86 27 87556262; fax: +86 27 87556262.

E-mail addresses: zghust@qq.com (G. Zhong), ssw636@hotmail.com (S. Wu).

Table 1

Chemical compositions of high silicon aluminum alloy (mass%).

Alloy	Si	Cu	Mg	Ni	Fe	Mn	Al
F0	20	2.0	0.4	1.0	2	0	Balance
F1	20	2.0	0.4	1.0	2	0.5	Balance

focuses in the research of manufacturing Al–Si alloy slurry with USV. Osawa et al. [13] studied the effect of USV on the morphology of primary intermetallic compounds of the alloys Al–xSi–4Fe ($x=6, 12, 18$). However, the shape-changing of Fe-bearing phases caused by USV and the mechanism of the USV on the morphology transformation of plate Fe-bearing phases are rarely reported till now.

In this paper, the effects of USV on the morphology of Fe-containing intermetallic compounds of high silicon aluminum alloy Al–20Si–2.0Fe–2.0Cu–0.4Mg–1.0Ni have been studied. The variations of Fe-containing intermetallic compounds with different USV time are analyzed. The transformation mechanism of Fe-containing phases with the complex role of USV and Mn addition is also discussed.

2. Experimental procedures

The installation of USV for high silicon Al–Si alloy in references [12] was employed in this experiment. The applied ultrasonic power in this study was 1.2 kW, and the frequency of USV was 20 kHz. Ultrasonic vibrator was composed of firmly connected transducer and amplitude made with titanium alloy.

The compositions of the alloys studied here were listed in Table 1, and Al–20Si–2.0Cu–0.4Mg–1.0Ni was the base alloy. The raw materials were Al–25.8% Si (mass%, the same in the following) and Al–10% Mn master alloy, commercial purity Al (99.7%), pure Cu (99.99%), pure Mg (99.9%), pure Ni (99.99%), and pure Fe (99.9%). The liquidus and the solidus temperature of this alloy which were determined by DSC, are about 702 °C and 533 °C respectively.

The alloy was melted in a resistance furnace at 820–850 °C with complex modification of 0.08% P in the form of Cu–14% P and 0.6% RE in the form of Al–15% RE, in which the RE was composed of 63% Ce and 36% La. Then the melt was held at 740–780 °C, and a metal cup was preheated to about 690 °C by the heating furnace simultaneously. Subsequently, about 600 g liquid metal was poured into the preheated metal cup. The USV was applied on the melt with the ultrasonic vibrator immersed into the melt 15–20 mm in depth, when the temperature of the liquid metal cooled down to about 715 °C. After the melt was treated with USV for certain time between 715 °C and 690 °C, the slurry with certain solid fraction obtained and then it was poured into the permanent mold of 8 mm in diameter. The application of USV ended at the temperature of about 690 °C. For comparison, conventional casting samples which formed at the temperature of 820 °C, were also made without USV.

The microstructure of the polished specimens was revealed by etching with 0.5% hydrofluoric acid solution, and examined with an Axiovert 200MAT optical microscope. In order to analyze the constituent phases and compositions, specimens were investigated using Quanta 200 environmental scanning electron microscope (SEM) fitted with an Energy Dispersive X-ray Spectroscopy (EDS) analysis system.

3. Results and discussion

3.1. Microstructure of high silicon aluminum alloy containing 2% Fe

Fig. 1 shows the typical as-cast microstructure of F0 alloy sample formed at the temperature of 820 °C in permanent mold, which is composed of primary Si (A), eutectic Si (B), dendritic compound (white C), acicular compound (bright white D), needle-like compound (light gray E), and a small amount of plate compound (light gray F). According to earlier studies of the authors [14], compound C, which can be refined to spherical particles in size of 1–2 μm by T6 heat treatment, is AlCuNi phase. And compound D is RE-containing five-element compound Al–Si–Cu–Ni–RE. An EDS analysis shows that the needle-like compound E and the plate compound F contain the same elements Al, Si and Fe atoms, as showed in Fig. 2. And the corresponding compositions contents of E and F are listed in Table 2. It was pointed out by related studies [4,6,7], that $\delta\text{-Al}_4\text{FeSi}_2$ phase commonly presented in high silicon aluminum alloy. As

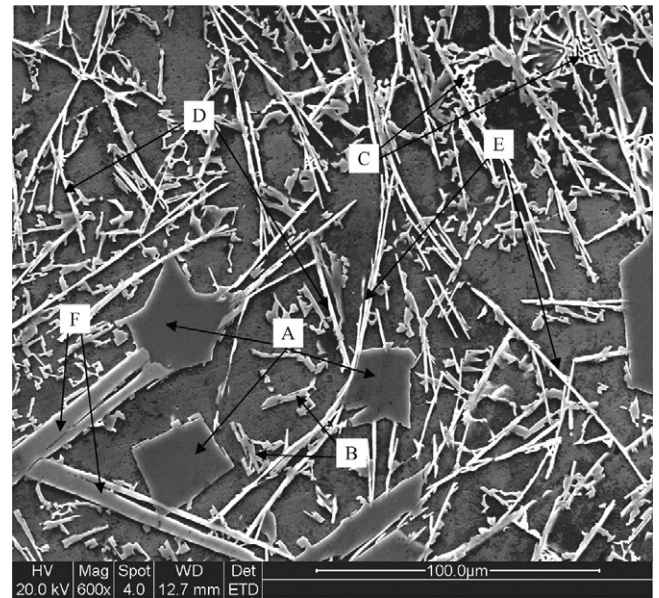


Fig. 1. SEM image of as-cast F0 alloy in traditional casting.

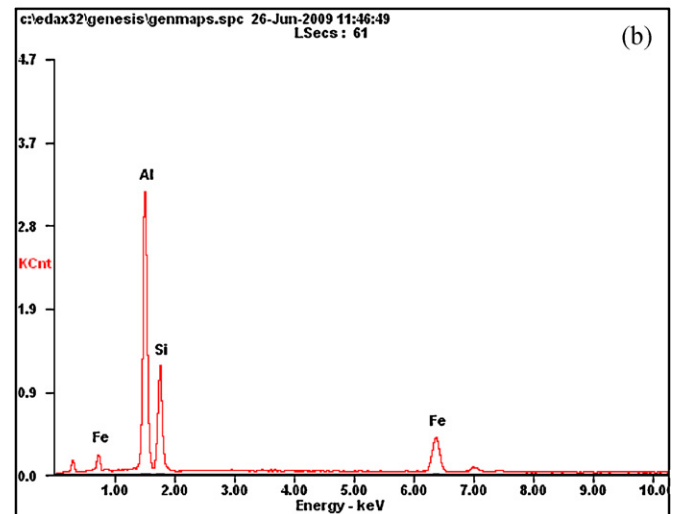
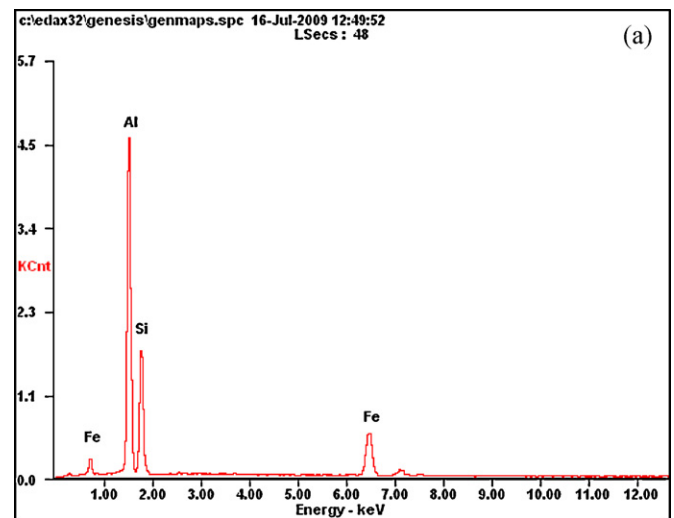


Fig. 2. EDS spectra of intermetallic compounds of F0 alloy in Fig. 1: (a) the result of light gray needle-like compound E; (b) the result of light gray plate compound F.

Table 2
EDS results (atom percent) of compounds of F0 alloy in liquid forming.

	Al	Si	Fe
Compound E	65.25	18.06	16.70
Compound F	53.10	31.00	15.90

Table 3
EDS results (atom percent) of Fe-containing phases of F0 alloy with USV.

Marks	Al	Si	Fe
a	53.10	31.00	15.90
b	51.76	30.90	17.33
c	52.25	31.06	16.70

can be seen from Table 2, the intermetallic compounds E and F should be monoclinic β -Al₅FeSi and tetragonal δ -Al₄FeSi₂ phases respectively. Based on the studies of Srivastava et al. and Huang et al. [5,7], the Fe-containing intermetallic compounds mainly consisted of metastable δ phase and a small amount of equilibrium β phase in the non-equilibrium solidification microstructure of the spray-deposited alloys Al-(18–25)Si–5Fe–X which experienced a big cooling rate about 10^3 – 10^5 °C s⁻¹. However, the opposite results can be seen in our study, that the Fe-containing phases mainly existed in form of needle-like β phase accompanied with a few plate δ phase of traditional casting F0 alloy. The different phenomena would be caused by the different solidification conditions of these two kinds of alloys. According to the Al–Si–Fe ternary phase diagram [6,15], the equilibrium solidification of Al–20Si–5Fe alloy starts with the formation of the δ phase at about 820 °C, followed by the formation of the primary Si phase below 700 °C. At the temperature below 610 °C, the previously δ phase transforms into the β phase with peritectic reaction $L + \delta\text{-Al}_4\text{FeSi}_2 \rightarrow \beta\text{-Al}_5\text{FeSi} + \text{Si}$, until the ternary eutectic reaction of α -Al, Si and β phases occurs at about 576 °C $L \rightarrow \alpha(\text{Al}) + \text{Si} + \beta\text{-Al}_5\text{FeSi}$. It is in favor of forming δ phase under the big cooling rate of rapid solidification. However, the average cooling rate of the cast iron mold used in this experiment was less than 10 °C s⁻¹, even at the sample surface was only about 20 °C s⁻¹. Therefore, the solidification in this mold would follow the sequence of equilibrium solidification events basically. As a result, most of the formed δ phase transformed into β phase via the peritectic reaction, and coarser β phase appeared for the longer solidification time compared with spray deposition.

3.2. Effects of ultrasonic vibration on the Fe-containing intermetallic compounds

The variations of Fe-containing phases of high silicon aluminum alloy with 2% Fe under different USV times are presented in Fig. 3. As can be seen from Fig. 3a pointed out by arrow, a large number of long needle-like β -Al₅FeSi phase in size of 100–200 μm distributed staggered in the matrix of F0 alloy without USV. However, when USV was applied for 60 s near the liquidus temperature of the alloy (715 °C), the β phase decreased significantly with some refined acicular β phase about 40–80 μm remained, and a large amount of block or polygonal intermetallic compound emerged (light gray in Fig. 3b designated by arrows, the gray particles were primary Si). The acicular β phase was further decreased and the block compound more refined and rounded with the effect of USV for 120 s as shown in Fig. 3c. Continuing to prolong the USV time to 180 s, only a few short acicular β phase existed in the matrix (Fig. 3d), but the block intermetallic compounds and the primary Si particles were coarser compared with those in Fig. 3c.

The long needle-like β phase was substituted by high volume fraction of block compound with the USV imposed on the F0 alloy. Therefore, the substitutes must also be Fe-containing compounds for the solution of Fe in solid Al is less than 0.05% [4]. The EDS analysis results which were measured for three random points of different block compounds of the alloys with USV, show that they all contain Al, Si and Fe atoms, as listed in Table 3. And the compositions contents indicate that they were basically the same as

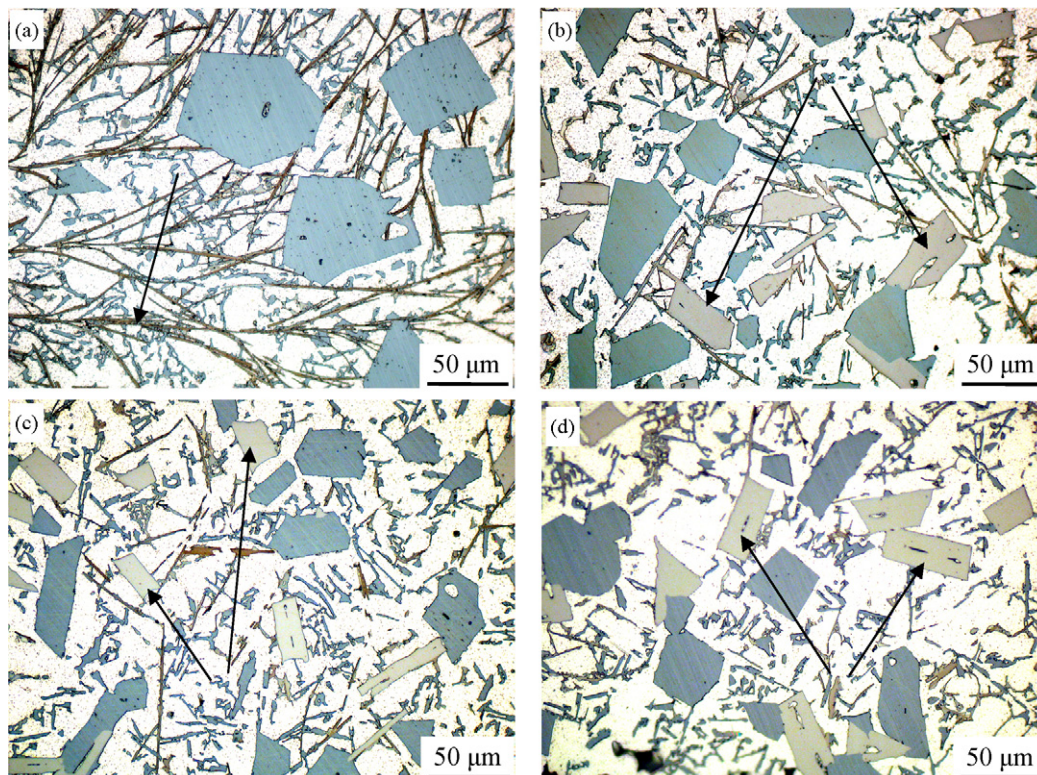


Fig. 3. The variations of Fe-bearing intermetallic compounds of F0 alloy with different USV time (images of samples as-cast): (a) 0 s; (b) 60 s; (c) 120 s; (d) 180 s.

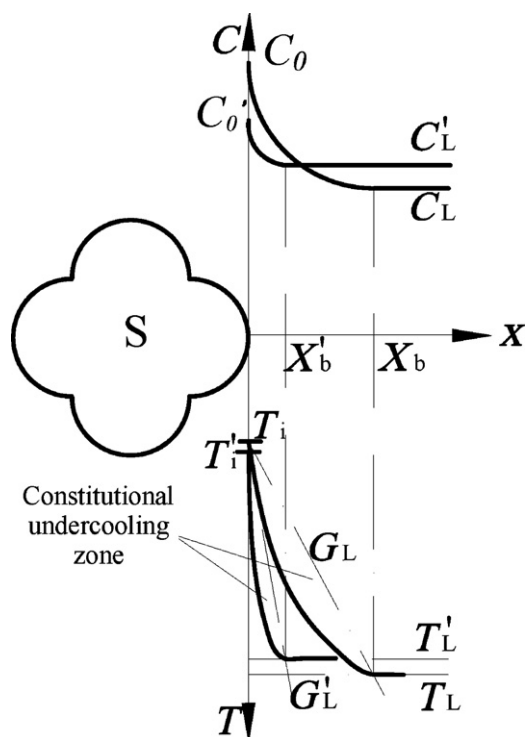


Fig. 4. Effect of USV on the solute and temperature distributions in front of a crystal.

the plate δ phase of F0 alloy without USV. So, the conclusion could be drawn that the forming of long needle-like β phase was suppressed, which was benefit to the formation of δ phase with the effect of USV on the alloy F0.

In the solidification process of this alloy, Fe atoms aggregate in the solidification front due to the large difference of solubility of Fe between liquid and solid Al, even a small amount of Fe in the alloy will cause harmful acicular β phase to form. It was verified [16] that the start-freezing temperature of β phase was variable, which decreased with decreasing iron content, increasing cooling rate, and increasing melt superheat temperature until it merges with the temperature of Al–Si eutectic reaction eventually. Among which, the Fe content has the greatest impact on the start-freezing temperature of β phase, which ascends sharply with the increasing iron content. And longer growth time is obtained because of enlarged forming temperature range, causing much coarser β phase. The same result could be observed through simulation of the β phase's start-freezing temperature of the alloys Al–20Si– x Fe ($x=1, 2, 5$) using JMatPro software, and the simulated results are 587.7 °C, 621 °C, 670 °C respectively.

Acoustic cavitation and streaming whose velocity is about $10\text{--}10^3$ times of that of the fluid thermal convection, will be produced by USV imposing on the metal melt [3,10–12,17,18]. A maximum speed of acoustic streaming about 1.37 m/s can be reached by this device for USV, based on theoretical calculations. And it plays an important role in homogenizing the solute distribution field and the temperature field of the melt, accelerating the heat and mass transfer, as well as dispersing the primary nuclei. The convection which speeds up uniform distribution of melt temperature, is strengthened by the combination of micro-flows generated by the broken of cavitation bubbles and macro-flows of molten melt induced by acoustic streaming. It is favorable to form homogenous solute distribution field and temperature field in the melt, with the application of USV on the melt before solidification, namely near the liquidus temperature. The effects of USV on the solute and temperature distribution of crystallization front are shown in Fig. 4. As can be seen, the solute concentration of crystal front decreased

from C_0 to C_0' , boundary layer thickness decreased from X_b to X_b' . The degree of constitutional undercooling also decreased as shown in Fig. 4 that the constitutional undercooling zone reduced from the area surrounded by curve $T_i\text{--}T_L$ and straight line G_L to that surrounded by curve $T_i'\text{--}T_L'$ and straight line G_L' . All of these are because of the lower level of solute concentration in solidification front, which caused by the acoustic streaming and micro-flow stirring in the melt.

Strong convection caused in the melt for the introduction of USV at about 715 °C, homogenized the solute distribution field and the temperature field of the melt. When the USV finished, the melt temperature was about 690 °C, and the semi-solid slurry with some pre-formed phases was obtained. The start-freezing temperature of β phase decreased in subsequent solidification process, for lower concentration degree of Fe atoms in the melt with USV. Moreover, a cooling rate about 10°C s^{-1} higher than that of traditional casting could be obtained because the forming temperature of semi-solid processing was about 130 °C lower than that of traditional casting. As a result, the start-freezing temperature of β phase further declined due to the higher cooling rate. Therefore, Fe-containing intermetallic compounds of the alloy with USV continue to form in the form of δ phase rather than acicular β phase.

The longer time USV imposing on the melt, the more uniform solute distribution, and the more difficult to form acicular β phase in the solidification process. As can be seen from Fig. 3, the needle-like β phases decreased remarkably (Fig. 3b) and a large number of block δ phases emerged in the matrix with the application of USV. The β phases kept on decreasing with the increasing time of USV, and there were only a small amount of β phases with USV treatment for 180 s (Fig. 3d). It can also be seen from Fig. 3, with USV time prolonged, the block δ phase, which was larger than 100 μm without USV as shown in Fig. 1, was refined to about 40–60 μm with the effect of USV for 60 s (Fig. 3b), and further refined to about 30 μm for 120 s (Fig. 3c). But coarse δ phase of larger than 50 μm acquired with the effect of USV for 180 s (Fig. 3d). The evenly distributed fields of temperature and solute of the melt generated by the effect of acoustic cavitation and acoustic streaming, not only promoted the formation of δ phase, but also inhibited the rapid growth of δ phase in a single direction bringing the refinement of particles. A part of refined needle-like β phase coexisted with coarse δ phase in the F0 alloy with USV 60 s, due to the influence of USV was not strong enough. And for 120 s, the effect of USV was sufficient for restricting the forming of β phase, the finest δ phase and only a small amount of β phase were obtained. Whereas, the δ phase grew and coarsened gradually for too long holding time under the USV for 180 s, though the acicular β phase continued to decrease for the further homogenous solute distribution.

3.3. Combined effects of ultrasonic vibration and Mn addition on the Fe-containing intermetallic compounds of high silicon aluminum alloy with 2% Fe

Fig. 5 shows the typical optical microstructures of F1 alloy containing 0.5% Mn with and without USV in as-cast state. As can be seen from Fig. 5a, that the intermetallic compounds of F1 alloy without USV were mainly composed of needle-like β phase and plate compound A (light gray). With the effect of USV for 120 s, the β phase basically eliminated and a large number of fine particles (such as the light gray compound B directed by the arrow) emerged with uniform distribution in the matrix, as shown in Fig. 5b. An EDS analysis shows that the plate compound A and the particles B contain the same elements Al, Si, Fe and Mn atoms, and the compositions contents of A and B are listed in Table 4. Based on the ratio of compositions, compound A is close to the formula $\text{Al}_4(\text{Fe},\text{Mn})\text{Si}_2$, and two kinds of compounds with the similar morphologies as B are close to the formula $\text{Al}_4(\text{Fe},\text{Mn})\text{Si}_2$ and $\text{Al}_5(\text{Fe},\text{Mn})\text{Si}$ respectively.

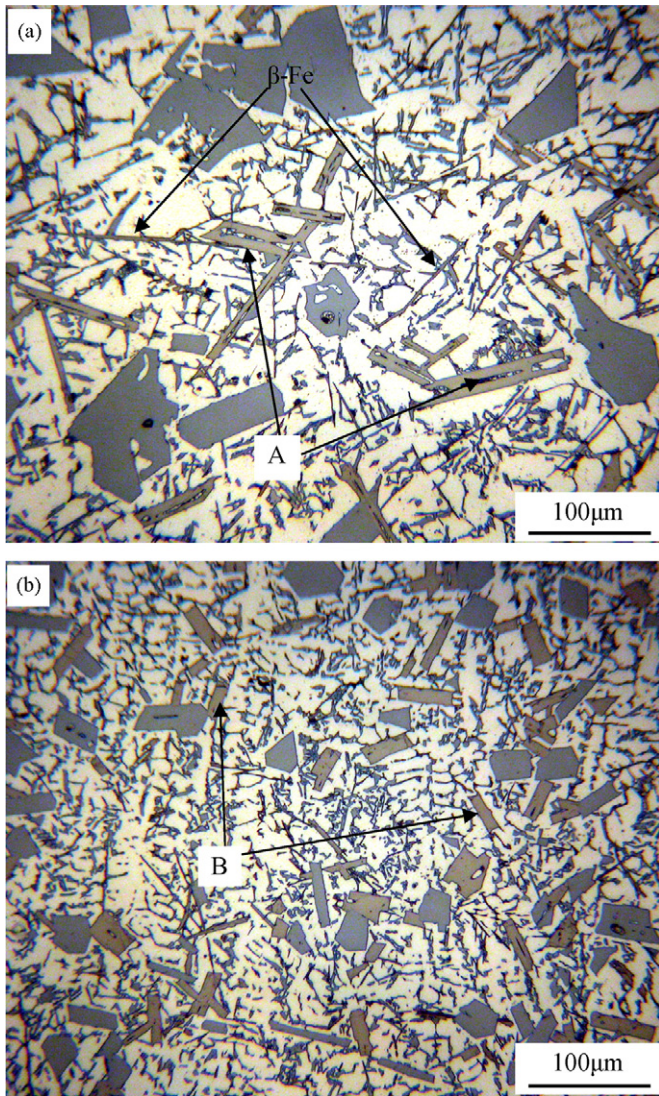


Fig. 5. Typical optical images of F1 alloy: (a) without USV; (b) with USV for 120 s.

Mn is commonly used to reduce the harmful effect of Fe, and the best neutralizing efficacy would be acquired with the addition as $Mn/Fe = 1/2$ [1,7]. It can be observed that the Fe-bearing intermetallic compounds were acicular β phase and plate $Al_4(Fe,Mn)Si_2$ phase in F1 alloy without USV (Fig. 5a), and more plate compound existed compared with the microstructure of F0 alloy without Mn (Fig. 1). The simulated result of the β phase's start-freezing temperature of the alloy $Al-20Si-2Fe-0.5Mn$ determined by JMatPro software was $611.5^\circ C$, about $10^\circ C$ lower than that of the alloy with the absence of Mn. As a result, the formation temperature range of δ phase was enlarged by about $10^\circ C$ for the lower start-freezing temperature of β phase with the addition of Mn. In this study, the relative content of Mn in F1 alloy was low ($Mn/Fe = 1/4$), which developed the positive role in joining the formation of $Al_4(Fe,Mn)Si_2$ phase. Both Mn and Fe are transition elements, and the positions in the lattices

of δ phase which are occupied by Fe atoms originally, are suitable to both Fe and Mn atoms. Therefore, Mn atoms were also involved in the formation of δ phase in the solidification process not with reactions but just a replacement of atoms due to the low Mn content, leading to coexistence of Fe and Mn atoms in the lattice of δ phase. As a result, only a small amount of Fe atoms were substituted by Mn atoms (illustrated by Table 4) forming the $Al_4(Fe,Mn)Si_2$ compounds. With the addition of Mn, on one hand, it enlarged the temperature range of forming δ phase which promoted the formation of $Al_4(Fe,Mn)Si_2$ compound and suppressed the rapid growth of it additionally. On the other hand, it was equivalent to increase the content of Fe in the alloy, so as to increase the amount of Fe-containing phases.

Fig. 5b shows that the forming of acicular β phase was almost repressed in F1 alloy with the combined effects of USV for 120 s and addition of 0.5% Mn, and the Fe-containing phases consisted of fine particles $Al_4(Fe,Mn)Si_2$ and $Al_5(Fe,Mn)Si$ in size of 20–30 μm . The effect of USV caused uniform distribution of temperature field and solute field, lowered the start-freezing temperature of β phase and promoted the formation of δ phase. Moreover, the temperature range of δ phase's formation was further extended with the addition of Mn which also involved in the formation of δ phase and β phase. Consequently, the small amount of acicular β phase shown in Fig. 3c transformed into fine $Al_5(Fe,Mn)Si$ phase, and was in coexistence with $Al_4(Fe,Mn)Si_2$ phase (Fig. 5b). It was found that $\beta-Al_5FeSi$ and $\delta-Al_4FeSi_2$ phases of spray-deposited alloys were difficult to distinguish due to their identical morphologies [7,19]. Therefore, it is not difficult to understand why $Al_4(Fe,Mn)Si_2$ and $Al_5(Fe,Mn)Si$ phases of F1 alloy with USV are in the similar morphologies.

4. Conclusions

- (1) A large amount of long needle-like $\beta-Al_5FeSi$ phase accompanied with a few plate $\delta-Al_4FeSi_2$ phase coexisted in the matrix of high silicon Al–Si alloy with 2% Fe in conventional casting process. However, Fe-containing intermetallic compounds of the alloy with USV continue to form in the form of δ phase rather than acicular β phases. The finest δ particles and only a small amount of β phase were obtained in the matrix of the Fe-containing alloy with USV for 120 s.
- (2) The effects of acoustic cavitation and acoustic streaming generated by USV which is imposed near the liquidus temperature of the alloy, homogenizes the solute distribution field and the temperature field of the melt. The mixing effect of USV on the solidification front lowers the concentration of Fe atoms, decreases the start-freezing temperature of β phase and promotes the formation of Fe-containing intermetallic compounds in the form of δ phase. The uniform distribution of solute in the melt restrains the rapid growth of δ phase in a single direction, causing the refinement of block δ phase.
- (3) The forming of acicular β phase of high silicon aluminum alloy was almost suppressed by adding 0.5% Mn and the effect of USV for 120 s, and the Fe-containing phases consisted of fine $Al_4(Fe,Mn)Si_2$ and $Al_5(Fe,Mn)Si$ particles in the size of 20–30 μm .

Acknowledgments

This work was funded by Project 50775086 supported by National Natural Science Foundation of China, and Project 2007AA03Z557 supported by the Hi-tech Research and Development Program of China. The authors would also like to express their appreciation to the Analytical and Testing Center, HUST.

Table 4

EDS results (atom percent) of Fe-containing phases of F1 alloy.

Marks	Al	Si	Mn	Fe
A	50.10	32.82	02.52	13.62
B	50.80	32.15	02.44	13.87
	66.40	16.02	02.90	14.68

References

- [1] F. Wang, J.S. Zhang, B.Q. Xiong, Y.G. Zhang, *Mater. Charact.* 60 (2009) 384–388.
- [2] Y.P. Wu, S.J. Wang, H. Li, X.F. Liu, *J. Alloys Compd.* 477 (2009) 139–144.
- [3] S.R. Yu, H.K. Feng, Y.L. Li, L.Y. Gong, *J. Alloys Compd.* 484 (2009), <http://www.sciencedirect.com/science/journal/09258388> 360–364.
- [4] N.A. Belov, A.A. Aksenov, D.G. Eskin, *Iron in Aluminum Alloys: Impurity and Alloying Element*, Taylor & Francis, London, 2002, pp. 265–270.
- [5] A.K. Srivastava, V.C. Srivastava, A. Gloter, S.N. Ojha, *Acta Mater.* 54 (2006) 1741–1748.
- [6] M. Rajabi, A. Simchi, M. Vahidi, P. Davami, *J. Alloys Compd.* 466 (2008) 111–118.
- [7] H.J. Huang, Y.H. Cai, H. Cui, J.F. Huang, J.P. He, J.S. Zhang, *Mater. Sci. Eng. A* 502 (2009) 118–125.
- [8] S. Seifeddine, S. Johansson, I.L. Svensson, *Mater. Sci. Eng. A* 490 (2008) 385–390.
- [9] N.A. Belov, D.G. Eskin, A.A. Aksenov, *Multicomponent Phase Diagrams: Applications for Commercial Aluminum Alloys*, Elsevier, Oxford, 2005, pp. 15–19.
- [10] H.K. Feng, S.R. Yu, Y.L. Li, L.Y. Gong, *J. Mater. Process. Technol.* 21 (2008) 330–335.
- [11] S.L. Zhang, Y.T. Zhao, X.N. Cheng, G. Chen, Q.X. Dai, *J. Alloys Compd.* 470 (2009) 168–172.
- [12] J.W. Zhao, S.S. Wu, P. An, Y.M. Mao, *Solid State Phenom.* 141–143 (2008) 767–771.
- [13] Y. Osawa, S. Takamori, T. Kimura, K. Minagawa, H. Kakisawa, *Mater. Trans.* 48 (2007) 2467–2475.
- [14] G. Zhong, S.S. Wu, H.W. Jiang, M. Sha, P. An, *Adv. Mater. Res.* 79–82 (2009) 1523–1526.
- [15] L.F. Mondolfo, *Aluminum Alloys: Structure and Properties*, Butterworths, London, 1976, pp. 471–475.
- [16] L. Anantha Narayanan, F.H. Samuel, J.E. Cruzleski, *Metall. Mater. Trans. A* 25 (1994) 1761–1773.
- [17] G.I. Eskin, *Ultrasonic Treatment of Light Alloy Melts*, Overseas Publishers Association, Russia, 1998, pp. 1–18.
- [18] Q. Ma, A. Ramirez, A. Das, *J. Cryst. Growth* 311 (2009) 3708–3715.
- [19] V.C. Srivastava, P. Ghosal, S.N. Ojha, *Mater. Lett.* 56 (2002) 797–801.